

Reversal symmetries for cyclic paths away from thermodynamic equilibriumJohn W. Biddle  and Jeremy Gunawardena **Department of Systems Biology, Harvard Medical School, Boston, Massachusetts, United States*

(Received 9 October 2019; revised manuscript received 8 April 2020; accepted 21 April 2020; published 16 June 2020)

If a system is at thermodynamic equilibrium, an observer cannot tell whether a film of it is being played forward or in reverse: any transition will occur with the same frequency in the forward as in the reverse direction. However, if expenditure of energy changes the rate of even a single transition to yield a nonequilibrium steady state, such time-reversal symmetry undergoes a widespread breakdown, far beyond the point at which the energy is expended. An explosion of interdependency also arises, with steady-state probabilities of system states depending in a complicated manner on the rate of every transition in the system. Nevertheless, in the midst of this global nonequilibrium complexity, we find that cyclic paths have reversibility properties that remain local, and which can exhibit symmetry, no matter how far the system is from thermodynamic equilibrium. Specifically, given any cycle of reversible transitions, the ratio of the frequencies with which the cycle occurs in one direction versus the other is determined, in the long-time limit, only by the thermodynamic force on the cycle itself, without requiring knowledge of transition rates elsewhere in the system. In particular, if there is no net energy expenditure on the cycle, then, over long times, the cycle occurrence frequencies are the same in either direction.

DOI: [10.1103/PhysRevE.101.062125](https://doi.org/10.1103/PhysRevE.101.062125)**I. INTRODUCTION**

Nonequilibrium systems are ubiquitous in nature, especially in biology. They are also notoriously difficult to deal with, lying largely beyond the scope of classical thermodynamics and the statistical mechanics developed in the 19th and early 20th centuries. In the 1960s, the biophysicist Terrell Hill introduced a diagrammatic method—essentially a graph—for analyzing individual biochemical entities, such as a membrane transporter complex, which operate stochastically under Markovian assumptions, away from thermodynamic equilibrium [1]. This approach was further developed in the 1970s in Jürgen Schnakenberg’s network theory [2]. One of the central ideas in their work was how cycles in the graph permitted macroscopic thermodynamic quantities, such as entropy production, to be related to stochastic mesoscopic quantities, such as fluxes between mesostates. These graphs could thereby be analyzed thermodynamically in spite of the global parametric complexity which arises away from thermodynamic equilibrium (below). For reasons that remain unclear, the use of such graphs then faded from sight for many years. They were not utilized for the major breakthroughs in nonequilibrium statistical mechanics which emerged in the 1990s in the work of Jarzynski, Crooks, and others [3–6]. More recently, as physicists have begun to build on these breakthroughs, the graph-based methods of Hill and Schnakenberg have come back into view [7,8], and the underlying Markov process representation has been widely adopted within the field of stochastic thermodynamics [9,10].

Independently of this physics tradition, an approach to timescale separation called the “linear framework” was

introduced in the biological literature in 2012, based on directed graphs with labeled edges [11]. The framework was originally applied to biochemical systems with large numbers of entities. For single entities, the approach may be seen, in a similar way to that of Hill and Schnakenberg, as a graph-based treatment of continuous-time, finite-state Markov processes. Vertices of the graph correspond to system states, edges to transitions between states, and labels to infinitesimal transition rates. Such a graph is not merely a description of the system but a mathematical object in its own right, in terms of which system properties can be calculated, irrespective of how far the system is from thermodynamic equilibrium [12]. We will use the linear framework here to show how graph cycles can retain local sequence-reversal symmetry, despite the global complexity that emerges away from thermodynamic equilibrium. We hope these results will reinforce the significance of Hill and Schnakenberg’s pioneering insights and draw further attention to the fertile area of study which lies between mathematics, physics, and biology.

II. THE LINEAR FRAMEWORK

As the linear framework has been described in several publications, we outline here only what is needed to set our results in context; for more background and history, see Refs. [11,13]; for further details and relevant applications, see Refs. [12,14–16]; for reviews, see Refs. [17,18]. Most of the assertions below are well known in stochastic thermodynamics, if not always with the same notation and terminology, and justifications can be found in the references cited above.

A linear framework graph, G , is a finite, directed graph with labeled edges and no self-loops. For the purposes discussed here, the vertices [often denoted $1, \dots, n$; the example in Fig. 1(a) uses a more explanatory naming convention]

*jeremy@hms.harvard.edu

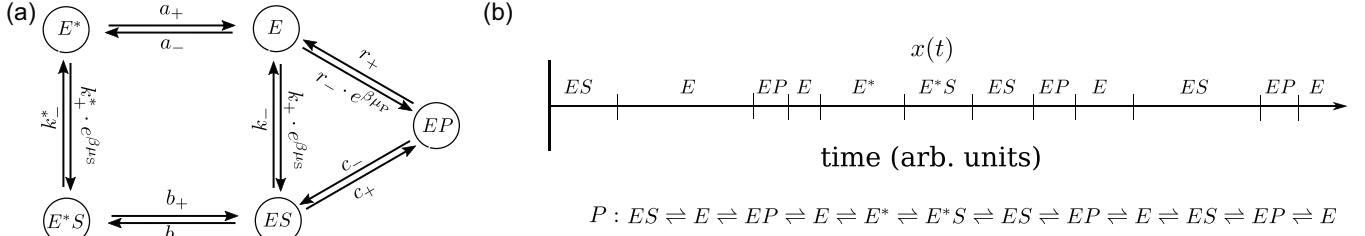


FIG. 1. (a) A linear framework graph describing a variant of the ligand-induced slow transition model of Ainslie *et al.* [19] of the biological phenomenon of kinetic cooperativity or “allokairy” [20]. An enzyme with two conformations, E and E^* , converts substrate S to product P only in its active conformation, E . The system is in thermal contact with a thermally uniform environment at reciprocal temperature β and is coupled to particle reservoirs for S and P , each held at a characteristic chemical potential, μ_S and μ_P , respectively. (b) A realization of the underlying Markov process gives rise to a trajectory $x(t)$. The vertical marks signify the jumps between the mesostates annotated above. The corresponding path of reversible transitions is shown below. Trajectories convey temporal information and provide the dwell time in each mesostate; paths convey only the order of transitions. Our results apply to paths rather than trajectories.

represent the states in which one might find a given realization of a system. We call the vertices “mesostates” to emphasize that while they refer to the configuration of the system and not to an ensemble, they are not microstates in the customary physics sense. The edges, denoted $i \rightarrow j$, represent transitions between mesostates; and the edge labels, denoted $\ell(i \rightarrow j)$, represent infinitesimal transition rates for an underlying Markov process and are positive quantities with dimensions of $[\text{time}]^{-1}$. If we let $X(t)$ denote the underlying Markov process at time t , then this process is specified by a conditional probability distribution $\Pr(X(t) = i | X(s) = j)$, where i and j are mesostates in G and $s < t$. With this notation,

$$\ell(i \rightarrow j) = \lim_{\Delta t \rightarrow 0} \frac{\Pr(X(t + \Delta t) = j | X(t) = i)}{\Delta t}. \quad (1)$$

Edge labels may include expressions which specify the interaction between mesostates and entities in the environment of the graph, such as particle reservoirs or thermal energy [Fig. 1(a)]. For our purposes here, as we will explain below, we can consider the labels to be symbolic constants representing positive real numbers.

The master equation of the Markov process describes the time evolution of mesostate probabilities, described by the column vector, $\mathbf{p}(t)$, where $p_i(t)$ is the probability that the system is in mesostate i at time t . This master equation can be obtained from G as

$$\frac{dp_i}{dt} = \sum_{j \neq i} [p_j \ell(j \rightarrow i) - p_i \ell(i \rightarrow j)].$$

Note that, since each edge has only one source vertex, each dp_i/dt is linear in the p 's. We can therefore represent the master equation as a linear differential equation,

$$\frac{d\mathbf{p}}{dt} = \mathcal{L}(G) \cdot \mathbf{p}(t), \quad (2)$$

where $\mathcal{L}(G)$ is the $n \times n$ Laplacian matrix of G [11, 13] and \mathbf{p} is the column vector of mesostate probabilities. It is easy to see that the column sums of $\mathcal{L}(G)$ are zero, which corresponds to the conservation of total probability. The relationship described above between graphs and Markov processes is quite general: given any continuous-time, finite-state Markov process, for which infinitesimal rates can be defined, there is a graph G for which Eq. (2) specifies the master equation [13].

For the applications considered here, we assume that the environmental variables affecting the rates do not change on the timescale over which the system is studied, and that temperatures and chemical potentials of the reservoirs are unaffected by any transitions that the system might undergo. We therefore treat the edge labels as symbolic constants.

This graph-based description of the Markov process allows effective calculation of quantities of interest whether or not the system is at thermodynamic equilibrium [Eqs. (3) and (4) below]. We outline the details of how this is done in the next section (Sec. III) before stating and proving our main results (Sec. IV).

Figure 1(a) gives an example of a linear framework graph used to model a biochemical system. We refer to this example to explain our approach. In Sec. V we present Gillespie simulations of the underlying system as an illustration of our results and how they might be employed experimentally.

III. PRELIMINARY RESULTS

A. Departure from equilibrium in the linear framework

1. Steady states and the Matrix-Tree theorem

We will assume from now on that G is strongly connected, so that any two vertices, i, j , are connected by a directed path of contiguous edges, $i = i_1 \rightarrow \dots \rightarrow i_k = j$. In this case, Eq. (2) has a unique steady state, \mathbf{p}^* . Equivalently, the kernel of the Laplacian matrix is one-dimensional, $\dim \ker \mathcal{L}(G) = 1$. A canonical basis element, $\rho(G) \in \ker \mathcal{L}(G)$, can be calculated from G through the Matrix-Tree theorem (MTT):

$$\rho_i(G) = \sum_{T \in \Theta_i(G)} \left[\prod_{j \rightarrow k \in T} \ell(j \rightarrow k) \right]. \quad (3)$$

Here, $\Theta_i(G)$ is the set of spanning trees of G rooted at vertex i . A spanning tree is a subgraph of G which includes all vertices of G (spanning) and has no cycles when edge directions are ignored (tree). It is rooted at i if i is the only vertex with no outgoing edges. Figure 2 shows two spanning trees rooted at the mesostate EP for the graph in Fig. 1(a).

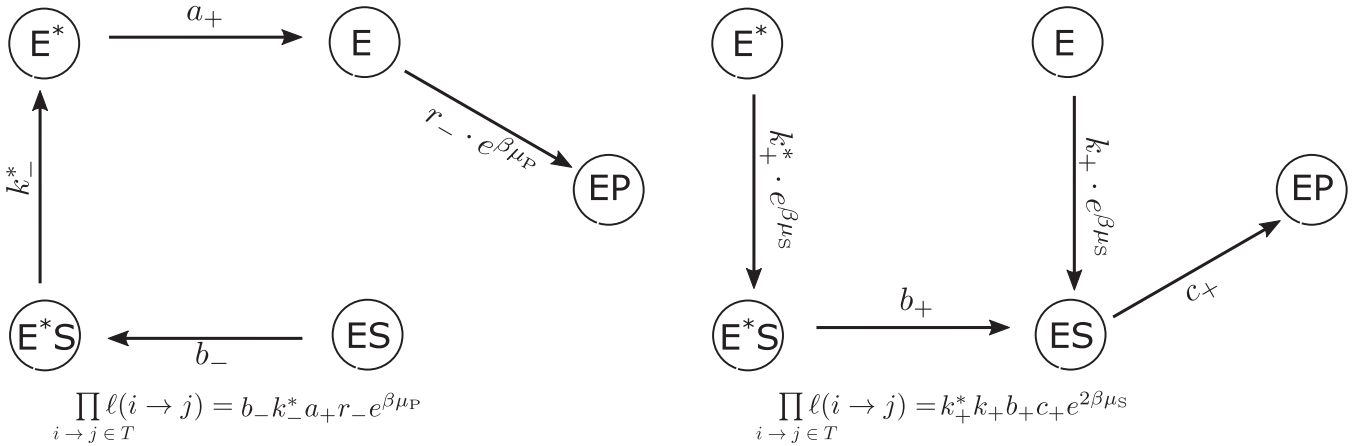


FIG. 2. Two of the 11 spanning trees rooted at vertex EP . Each tree contributes a term to the expression in Eq. (3), as shown below each tree.

Since $\mathbf{p}^* = \lambda \rho(G)$, for some scalar $\lambda \in \mathbb{R}^+$, it follows from the conservation of probability that

$$p_i^* = \frac{\rho_i(G)}{\rho_1(G) + \dots + \rho_n(G)}. \quad (4)$$

Equation (4) expresses steady-state probabilities in terms of the edge labels, through Eq. (3), and can be applied to a system maintained arbitrarily far from thermodynamic equilibrium. The MTT is not required for our main result, but, in conjunction with Eq. (7) below, it illustrates the dramatic increase in global parametric complexity that arises away from equilibrium. Equation (3) shows that the steady-state probability of each mesostate becomes dependent in a complicated way on edge labels throughout the graph. The MTT, first proved in this form by Tutte [21], was known to Hill [1] and Schnakenberg [2] but then seems to have disappeared from view; for its convoluted history across many disciplines and a proof, see Ref. [13].

2. Thermodynamic equilibrium

If a system can reach thermodynamic equilibrium, then it must obey the principle of detailed balance. This principle holds at all scales from elementary to mesoscopic systems: observing a trajectory over time, transitions from configuration i to j and from configuration j to i will happen with equal frequency, however coarse- or fine-grained the conceptions of i and j may be [22]. Detailed balance arises from time-reversal symmetry of the underlying fundamental laws of physics [23].

Let us denote the flux along the edge $i \rightarrow j$, or $p_i \ell(i \rightarrow j)$, by $J_{i \rightarrow j}$; this is proportional to the average rate at which the system makes the transition $i \rightarrow j$. In order to satisfy detailed balance, the graph must be reversible: given the edge $i \rightarrow j$, there must exist an edge $j \rightarrow i$, which represents the reverse transition (and not merely an alternative way of returning from j to i). It must also be the case that the forward and reverse fluxes equal each other, so that the net flux vanishes, $J_{i \rightarrow j} - J_{j \rightarrow i} = 0$. Equivalently,

$$\frac{p_j^*}{p_i^*} = \frac{\ell(i \rightarrow j)}{\ell(j \rightarrow i)}. \quad (5)$$

For systems that can reach equilibrium in contact with one or more reservoirs (of particles, heat, etc.) a free energy, $F(i)$, can be associated with each mesostate, i . This gives a physical interpretation for the ratios of transition rates,

$$\log \left[\frac{\ell(i \rightarrow j)}{\ell(j \rightarrow i)} \right] = \beta \Delta F_{ij}, \quad (6)$$

where $\Delta F_{ij} = F(i) - F(j)$. This identification goes back to Hill [1] and Schnakenberg [2], and we discuss below [Eq. (10)] how it has been extended to nonequilibrium systems.

Equation (5) leads to an alternative basis element $\mu(G) \in \ker \mathcal{L}(G)$. Choose a reference mesostate in G , usually taken to be the mesostate indexed by 1. Given any path of reversible edges from 1 to a given mesostate i , $1 = i_1 \rightleftharpoons i_2 \rightleftharpoons \dots \rightleftharpoons i_{k-1} \rightleftharpoons i_k = i$, let

$$\mu_i(G) = \left[\frac{\ell(i_1 \rightarrow i_2)}{\ell(i_2 \rightarrow i_1)} \right] \dots \left[\frac{\ell(i_{k-1} \rightarrow i_k)}{\ell(i_k \rightarrow i_{k-1})} \right]. \quad (7)$$

It is clear from Eq. (5) that $\mu_i(G)$ does not depend on the chosen path from 1 to i and that, because $\dim \ker \mathcal{L}(G) = 1$ and $\mu_1(G) = 1$, $p_i^* \mu_i(G) = p_i^*$. It follows that $\mu(G) \in \ker \mathcal{L}(G)$ and that $\rho_1(G) \mu(G) = \rho(G)$. The denominator of Eq. (4) is then proportional to the partition function for the relevant ensemble of statistical mechanics. It also provides an analog of the partition function for a nonequilibrium system.

3. Nonequilibrium complexity and the breakdown of detailed balance

On the other hand, a system may be maintained away from thermodynamic equilibrium. The comparison between $\mu(G)$, at thermodynamic equilibrium, and $\rho(G)$, away from equilibrium, is instructive. With the former, Eq. (7) shows that it is sufficient to take any single path in G to a given mesostate to calculate its steady-state probability using Eq. (4). With the latter, when detailed balance is broken, not only do steady-state probabilities become path dependent, every path in G makes a contribution to them and the MTT in Eq. (3) provides the bookkeeping for this calculation. The combinatorial explosion coming from enumerating all rooted spanning trees

can be super-exponential in the size of G [14], and the steady-state probability of a mesostate can come to depend in an extremely complicated manner on all the labels in G . The graph-based approach here provides a vivid demonstration of the profound difference between equilibrium and nonequilibrium states.

The impact of nonequilibrium path dependency is felt globally even if energy expenditure is limited and local. If we take a graph G that obeys detailed balance, and perturb even a single edge label, $\ell(i \rightarrow j)$, so as to break detailed balance, the resulting change in \mathbf{p}^* due to Eq. (3) leads to a widespread breakdown of detailed balance [Eq. (5)] even at edges whose labels retain their equilibrium values. This point is clearly illustrated in the simulations undertaken below (Sec. V) of the example in Fig. 1(a).

A system might be maintained away from equilibrium through contact with multiple reservoirs at different temperatures or chemical potentials. This is common in biological systems, from molecular motors which exploit a chemical potential difference between ATP, on the one hand, and ADP and inorganic phosphate, P_i , on the other, to enzymes which operate in the presence of a chemical potential difference between substrate and product, as in the example in Fig. 1(a). Alternatively, chemical or other energy may be consumed by the system itself and then dissipated to the environment, as in the case of active matter. We note that either kind of nonequilibrium system can be treated within the linear framework.

B. Cycles and affinities

An equivalent condition to the statement of detailed balance in Eq. (5) can be given in terms only of the edge labels. Consider any cycle of reversible edges, $i_1 \rightleftharpoons i_2 \rightleftharpoons \dots \rightleftharpoons i_{m-1} \rightleftharpoons i_m = i_1$. Cycles need not be simple: the same mesostate may appear more than once, with more than one index, in the numbered list. At thermodynamic equilibrium, the product of the labels in one direction around the cycle equals the product in the other direction,

$$\ell(i_1 \rightarrow i_2) \cdots \ell(i_{m-1} \rightarrow i_m) = \ell(i_m \rightarrow i_{m-1}) \cdots \ell(i_2 \rightarrow i_1). \quad (8)$$

Equation (8) makes clear that, if G can reach thermodynamic equilibrium, the edge labels are not independent quantities. The label ratios on the edges of any rooted spanning tree form a set of independent parameters, in terms of which all other label ratios can be determined using Eq. (8) [14]. If a graph is at thermodynamic equilibrium, flux balance as given by Eq. (5) and the cycle condition as given by Eq. (8) are equivalent statements [16].

For any cycle C as described above, there is an affinity $\tilde{A}(C)$ associated with the cycle, defined as the logarithm of the ratio of the corresponding terms in Eq. (8):

$$\tilde{A}(C) = \log \left[\frac{\ell(i_1 \rightarrow i_2) \cdots \ell(i_{m-1} \rightarrow i_m)}{\ell(i_2 \rightarrow i_1) \cdots \ell(i_m \rightarrow i_{m-1})} \right]. \quad (9)$$

It follows from Eq. (8) that for a system at thermodynamic equilibrium $\tilde{A}(C) = 0$ for all cycles. We follow Schnakenberg [2] and Hill [1] in this definition of the affinity.

The affinity of a cycle has a natural thermodynamic interpretation, which arises from an extension of Eq. (6) to systems maintained away from equilibrium. For a reversible edge, $i \rightleftharpoons j$,

$$\log \left[\frac{\ell(i \rightarrow j)}{\ell(j \rightarrow i)} \right] = \Delta S^{\text{res}} + \Delta S_{ji}^{\text{sys}}. \quad (10)$$

Here the right-hand side represents the total change in entropy in all reservoirs when the system makes the transition from i to j and the internal entropy difference between mesostate j and mesostate i . Equation (10) is referred to as ‘‘local detailed balance,’’ which can be justified under a broad range of conditions [24,25]. To take an example from the graph in Fig. 1(a), the pair of substrate binding and unbinding transitions would satisfy

$$\log \left[\frac{\ell(E \rightarrow ES)}{\ell(ES \rightarrow E)} \right] = \beta(F(E) - F(ES) + \mu_S).$$

It follows readily from Eq. (10) that the affinity of a cycle is given by

$$\tilde{A}(C) = \Delta S^{\text{res}}, \quad (11)$$

where ΔS^{res} is the total entropy produced in the reservoirs by one completion of the cycle.

In considering the affinity, $\tilde{A}(C)$, of cycle C , it is helpful to keep in mind that only minimal cycles contribute to it. A cycle is minimal if it contains no repeated mesostates and at least three mesostates. For instance, for the graph in Fig. 1(a), the cycle $E \rightleftharpoons ES \rightleftharpoons E$ is not minimal. It is a simple instance of an ‘‘excursion’’ which takes a path from E to ES and then returns along the reverse path. There is no net energy expenditure along such excursions—in this case a substrate molecule, S , is taken from its reservoir and then returned to it—and the affinity is zero. The only parts of a cycle which contribute to the affinity are those corresponding to minimal cycles.

As we have defined it, a cycle specifies its starting mesostate, but the cycle properties described above are independent of the starting point. The following notation will therefore be helpful. Given a cycle $C: i_1 \rightleftharpoons i_2 \rightleftharpoons \dots \rightleftharpoons i_{m-1} \rightleftharpoons i_m = i_1$, let $C(i_j)$, where $1 \leq j \leq m$, denote the cycle with the same order of transitions starting at mesostate i_j , $C(i_j): i_j \rightleftharpoons i_{j+1} \rightleftharpoons \dots \rightleftharpoons i_{m-1} \rightleftharpoons i_1 \rightleftharpoons i_2 \rightleftharpoons \dots \rightleftharpoons i_{j-1} \rightleftharpoons i_j$. It follows that $C(i_1) = C(i_m) = C$. Let $\{C\}$ denote the set of cycles having the same cyclic order of transitions, $\{C\} = \{C(i_1), C(i_2), \dots, C(i_{m-1})\}$. Note that the cycle condition in Eq. (8) and the affinity in Eq. (9) are both well defined as properties of $\{C\}$.

IV. MAIN RESULT: REVERSAL SYMMETRY OF CYCLES

We need some further notation to state our main result. Let $P: i_1 \rightleftharpoons i_2 \rightleftharpoons \dots \rightleftharpoons i_{m-1} \rightleftharpoons i_m$ be any path of reversible edges in a graph G , where $m > 2$. Consider observing a trajectory of the underlying Markov process [Fig. 1(b)]. Denote the number of times that P occurs on the trajectory by $n[P, x(t)]$. It is important that all the mesostates on the path are observed in the specified order without deviations. For the example trajectory in Fig. 1(b) and for the path $P: ES \rightleftharpoons EP \rightleftharpoons E$,

$n[P, x(t)] = 2$, while for the cycle $P: E \rightleftharpoons ES \rightleftharpoons EP \rightleftharpoons E$, $n[P, x(t)] = 1$.

Let $\text{Pr}(P)$ denote the probability that the Markov process, having reached the initial mesostate i_1 , will subsequently go through the transitions in P in exactly the specified order without deviation. Since G is strongly connected with positive labels, we can appeal to the ergodic theorem for Markov processes [26] to interpret the probability in frequentist terms,

$$\text{Pr}(P) = \lim_{t \rightarrow \infty} \frac{n[P, x(t)]}{n[i_1, x(t)]}, \quad (12)$$

where the denominator is the number of times in which the starting mesostate, i_1 , is observed along the trajectory.

Given a cycle $C: i_1 \rightleftharpoons i_2 \rightleftharpoons \dots \rightleftharpoons i_{m-1} \rightleftharpoons i_m = i_1$ let C^r denote the reverse cycle, $C^r: i_m \rightleftharpoons i_{m-1} \rightleftharpoons \dots \rightleftharpoons i_2 \rightleftharpoons i_1 = i_m$. We can easily extend the definition to cycle sets by defining $\{C\}^r = \{C^r\}$. Along a trajectory, the same cyclic order of transitions may be observed starting at any mesostate, so we can define $n[\{C\}, x(t)]$ to be

$$n[\{C\}, x(t)] = n[C(i_1), x(t)] + \dots + n[C(i_{m-1}), x(t)].$$

Theorem: For any connected reversible graph, any cycle $C: i_1 \rightleftharpoons i_2 \rightleftharpoons \dots \rightleftharpoons i_{m-1} \rightleftharpoons i_m = i_1$ of reversible edges in G and any mesostate i_j on C :

$$\lim_{t \rightarrow \infty} \frac{n[C(i_j), x(t)]}{n[C(i_j)^r, x(t)]} = \lim_{t \rightarrow \infty} \frac{n[\{C\}, x(t)]}{n[\{C^r\}, x(t)]} = e^{\tilde{A}(C)}.$$

The proof of this requires a couple of steps. The first step is to calculate probabilities. Under the conditions of the theorem, we claim that

$$\frac{\text{Pr}(C(i_j))}{\text{Pr}(C(i_j)^r)} = e^{\tilde{A}(C)}. \quad (13)$$

To see this, note that, conditional on the system being in mesostate i_1 , the probability that its next transition will be to state i_2 is given by

$$\frac{\ell(i_1 \rightarrow i_2)}{\sum_{i_1 \rightarrow j} \ell(i_1 \rightarrow j)}, \quad (14)$$

where the sum in the denominator is over all outgoing edges in G from i_1 . Let us denote this latter quantity, for a given mesostate i , by $\mathcal{Z}(i) = \sum_{i \rightarrow j} \ell(i \rightarrow j)$, so that $\mathcal{Z}(i_1)$ gives the denominator in Eq. (14). Since the probability in Eq. (14) leads to mesostate i_2 , the calculation can be continued to determine the probability, conditional on starting in mesostate i_1 , that the system makes the transition from i_1 to i_2 followed by the transition from i_2 to i_3 :

$$\frac{\ell(i_1 \rightarrow i_2)}{\mathcal{Z}(i_1)} \cdot \frac{\ell(i_2 \rightarrow i_3)}{\mathcal{Z}(i_2)}.$$

It follows by induction that, conditional on starting in mesostate i_1 , the probability that the next $m-1$ transitions will be as specified by cycle C is given by

$$\frac{\prod_{k=1}^{m-1} \ell(i_k \rightarrow i_{k+1})}{\prod_{k=1}^{m-1} \mathcal{Z}(i_k)}. \quad (15)$$

The equivalent expression for C^r is given by

$$\frac{\prod_{k=2}^m \ell(i_k \rightarrow i_{k-1})}{\prod_{k=2}^m \mathcal{Z}(i_k)}. \quad (16)$$

Hence, taking the ratio of Eq. (15) by Eq. (16) and recalling that $i_1 = i_m$ and the definition of affinity in Eq. (9), we see that

$$\frac{\text{Pr}(C)}{\text{Pr}(C^r)} = \left[\frac{\mathcal{Z}(i_m)}{\mathcal{Z}(i_1)} \right] \frac{\prod_{k=1}^{m-1} \ell(i_k \rightarrow i_{k+1})}{\prod_{k=2}^m \ell(i_k \rightarrow i_{k-1})} = e^{\tilde{A}(C)}. \quad (17)$$

This final value is independent of the starting mesostate i_1 , from which the claim made in Eq. (13) follows.

We can now use Eq. (12) to interpret probabilities in terms of cycle counts. We see that

$$\text{Pr}(C(i_j)) = \lim_{t \rightarrow \infty} \frac{n[C(i_j), x(t)]}{n[i_j, x(t)]} \quad \text{and}$$

$$\text{Pr}(C(i_j)^r) = \lim_{t \rightarrow \infty} \frac{n[C(i_j)^r, x(t)]}{n[i_j, x(t)]}.$$

It follows from Eq. (13) that both of these quantities are nonzero and, therefore,

$$\begin{aligned} \lim_{t \rightarrow \infty} \frac{n[C(i_j), x(t)]}{n[C(i_j)^r, x(t)]} &= \lim_{t \rightarrow \infty} \frac{n[C(i_j), x(t)]/n[i_j, x(t)]}{n[C(i_j)^r, x(t)]/n[i_j, x(t)]} \\ &= \frac{\text{Pr}(C(i_j))}{\text{Pr}(C(i_j)^r)} = e^{\tilde{A}(C)}. \end{aligned} \quad (18)$$

This establishes part of the theorem.

The remaining part comes from the following observation, whose proof is elementary. If functions $a_j(t)$ and $b_j(t)$ are defined for $1 \leq j \leq m$ and satisfy $\lim_{t \rightarrow \infty} a_j(t)/b_j(t) = \alpha$ for each j , then

$$\lim_{t \rightarrow \infty} \frac{a_1(t) + \dots + a_m(t)}{b_1(t) + \dots + b_m(t)} = \alpha. \quad (19)$$

Taking $a_j(t) = n[C(i_j), x(t)]$ and $b_j(t) = n[C(i_j)^r, x(t)]$ and using Eq. (18) completes the proof of the theorem.

V. SIMULATIONS

Figure 3 illustrates the properties of cyclic paths for the allokaairy example in Fig. 1. Three minimal cycles (Sec. III) are shown color coded in Fig. 3(a). The system was simulated for three scenarios. Case i: thermodynamic equilibrium, with $\mu_S = \mu_P$. Case ii: the system is driven from equilibrium by a difference in chemical potential between substrate and product, $\mu_S > \mu_P$, so that the reaction favors product formation. The only difference from the equilibrium case is a difference in the rate of product rebinding, for the edge $E \rightarrow EP$. Case iii: two different forces drive the system away from equilibrium. As in case ii, $\mu_S > \mu_P$. Additionally, rather than merely being different conformations, E^* and E are treated as phosphorylated and nonphosphorylated forms of the enzyme, respectively. The process of phosphorylation and dephosphorylation is driven by ATP hydrolysis, with the system in contact with reservoirs of ATP, ADP, and P_i . Cycles 2 and 3 experience the difference in chemical potential given by $\mu_{\text{ATP}} - \mu_{\text{ADP}} - \mu_{P_i}$. The temperature and chemical potentials used in the simulations, as well as the transition rates themselves, are provided as Supplemental Material [27].

We carried out Gillespie simulations for this model in the three different scenarios and recorded the resulting edge fluxes and cycle occurrence statistics. In case i, the system is at thermodynamic equilibrium. It is coupled to two particle

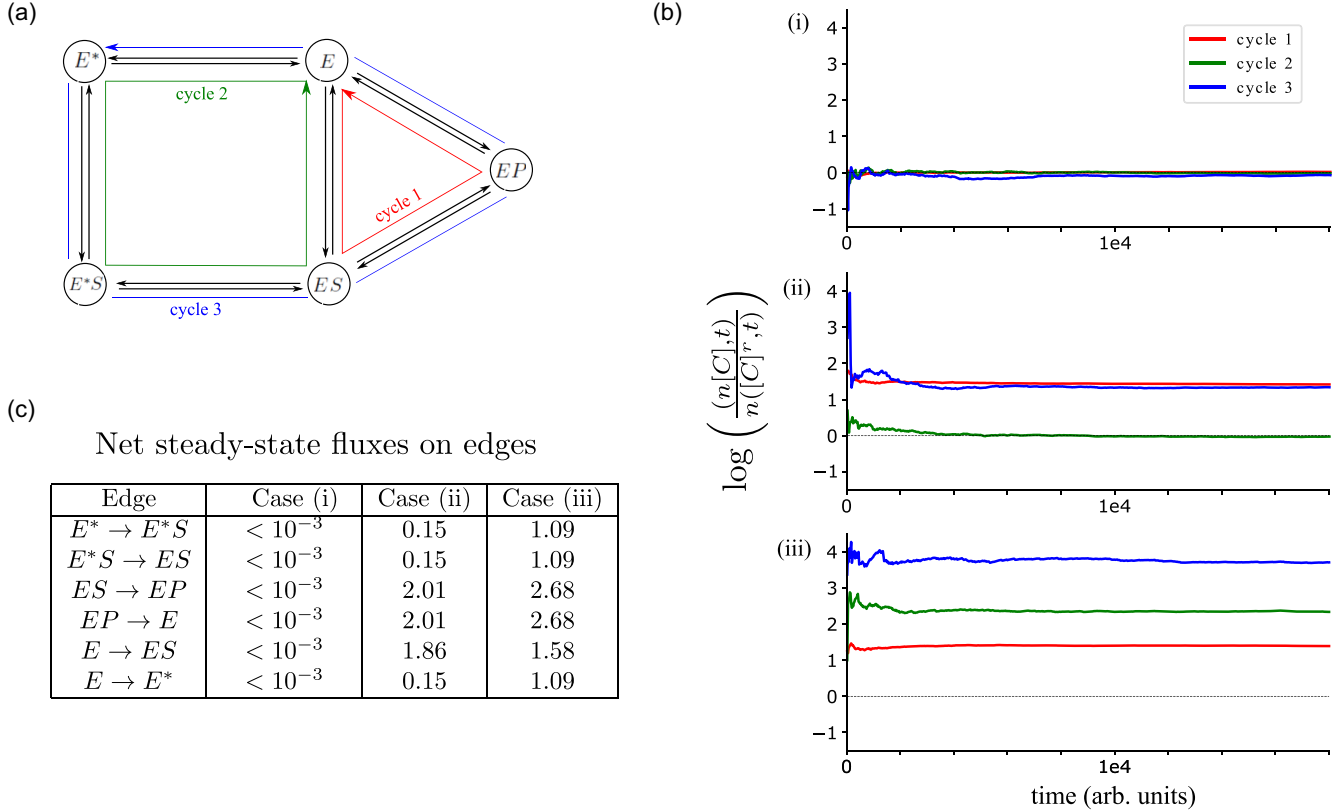


FIG. 3. Illustration of symmetry properties of cyclic paths. (a) The example graph from Fig. 1 is shown with three cycles color coded. The text explains the three scenarios which were studied. (b) Logarithmic plots of the reversibility ratio in the theorem, with time, t , in arbitrary units, for each scenario, as annotated to the top left of each plot. (c) The net flux, $J_{i \rightarrow j} - J_{j \rightarrow i}$ associated with each pair of forward and reverse transitions, $i \rightleftharpoons j$, is shown for each scenario. The first column gives the edge $i \rightarrow j$ in the direction of net flux. [The values for case i denote absolute values.] The text discusses the flux patterns.

reservoirs, of S and P , whose chemical potentials are equal: $\mu_S = \mu_P$. In this case, all net fluxes vanish [Fig. 3(c), column 2] and all cycle reversibility ratios tend to unity [Fig. 3(b), top]. In case ii, $\mu_S > \mu_P$ so that the reaction favors product formation. Cycles 1 and 3 thus have affinity $\tilde{A}(C) = \beta(\mu_S - \mu_P)$, while cycle 2 has zero affinity [Fig. 3(b), middle]. In case iii, cycles 2 and 3 are driven by ATP-dependent phosphorylation. The affinity of cycle 3 becomes $\tilde{A}(C_3) = \beta(\mu_{ATP} + \mu_S - \mu_{ADP} - \mu_{P_i} - \mu_P)$, and cycle 2 acquires a nonzero affinity as well, $\tilde{A}(C_2) = \beta(\mu_{ATP} - \mu_{ADP} - \mu_{P_i})$. In both nonequilibrium scenarios all reversible edges in the graph acquire net fluxes [Fig. 3(c), columns 3 and 4]. At steady state, the net flux from E to E^* , from E^* to E^*S and from E^*S to ES must be equal, as must the net flux from ES to EP and from EP to E , while the net flux from E to ES gives the difference between these two amounts (in case iii the slight discrepancy in flux balance arises from rounding error).

Case ii differs from the equilibrium case i only in one rate, $\ell(E \rightarrow EP)$. Nevertheless, net fluxes appear at all reversible edges. In fact, cases ii and iii are difficult to distinguish by an examination of net fluxes alone. The reversal ratio plots, however, look quite different. In case i, symmetry is preserved for all cycles. In case ii, cycle 2 retains its reversal symmetry, while it is broken for cycles 1 and 3 to the same extent. In

case iii, reversal symmetry is broken for all cycles, each to a different extent.

VI. DISCUSSION

The principle of detailed balance at equilibrium is stated succinctly by ter Haar: “at equilibrium the number of processes destroying situation A and creating situation B will be equal to the number of processes producing A and destroying situation B” [22]. Hence, the observation of any process happening more frequently than its reverse is confirmation that the system is away from equilibrium. However, as Fig. 3(c) clearly shows, the breakdown of this symmetry in a nonequilibrium system is so pervasive that a single transition that is driven away from equilibrium can disrupt the balance between every pair of forward and reverse transitions. Furthermore, it can make the steady-state probability of every mesostate dependent on all the rates in the system. Even for a simplified system like the one in Fig. 1(a), Eq. (3) shows that one must enumerate 55 spanning trees (Fig. 2), each containing four factors, to compute the nonequilibrium steady-state probabilities of the system. By contrast, the probabilities can be computed at equilibrium from four ratios of rates. Notwithstanding this path-dependent complexity, cyclic paths on which there is no net energy expenditure retain a

remarkable symmetry: for long trajectories, one can expect to observe such a cycle and its reverse with the same frequency. Furthermore, the extent to which this symmetry is broken for a cycle which is driven away from equilibrium is a function only of the affinity of the cycle, irrespective of thermodynamic forces acting elsewhere in the system.

As noted in the Introduction, the use of graph cycles to study the thermodynamics of Markov processes goes back to the work of Hill and Schnakenberg. Schnakenberg, following Hill, introduced a measure of cycle flux, which, together with the cycle affinity [Eq. (9)], allows the overall entropy production to be determined [2]. These cycle fluxes are distinct from the cycle counts considered here. Hill introduced a way of counting cycles along a trajectory and analyzed the fluctuations in this quantity [28,29]. Jiang *et al.* subsequently provided rigorous proofs of Hill's observations as well as several other results [30]. The cycle count definitions in these papers are different from ours. Hill and Jiang *et al.* focus only on minimal cycles, as defined in Sec. III, and they count cycle completions, allowing for excursions away from the cycle, by recursively removing cycles from a path. For them, the trajectory in Fig. 1(b) contains only the completed cycles $ES \rightleftharpoons E \rightleftharpoons E^* \rightleftharpoons E^*S \rightleftharpoons ES$ and $ES \rightleftharpoons EP \rightleftharpoons E \rightleftharpoons ES$. The resulting asymptotic counts over long trajectories are entirely appropriate for determining fluxes on edges and calculating overall entropy production. If the asymptotic count for a cycle is equal to the asymptotic count for the reversed cycle, and this is true for all minimal cycles in the graph, then the system is at thermodynamic equilibrium [30, Theorem 2.2.10].

In contrast, we consider any cycle, and our way of counting cycle occurrences, rather than cycle completions, does not allow excursions away from the cycle. Accordingly, we find the second cycle given above in the trajectory in Fig. 1(b), counted once with the given starting mesostate. We do not count any occurrences of the first cycle given above, but we do count single occurrences of four other cycles: $EP \rightleftharpoons E \rightleftharpoons E^* \rightleftharpoons E^*S \rightleftharpoons ES \rightleftharpoons EP$, $E \rightleftharpoons E^* \rightleftharpoons E^*S \rightleftharpoons ES \rightleftharpoons EP \rightleftharpoons E$, $EP \rightleftharpoons E \rightleftharpoons ES \rightleftharpoons EP$, and $E \rightleftharpoons ES \rightleftharpoons EP \rightleftharpoons E$. The asymptotic ratio of forward cycle count compared to reversed cycle count provides local information about net energy expenditure on that cycle, irrespective of whether or not there is energy expenditure elsewhere in the system.

The behavior under sequence reversal of our cycle counts, as given by the theorem, is suggestive of a symmetry.

Nonequilibrium fluctuation theorems in the Markov process setting reveal a striking symmetry in the large deviation function, or cumulant generating function, for asymptotic fluctuations in stochastic quantities like fluxes (“currents”) or entropy production [6,7,31,32]. The reversal symmetry we find pertains only to the mean of the cycle occurrence distribution. It is conceivable that this could be recovered in some way from the more general symmetries of fluctuation theorems, but we know of no way to do so at present.

As Hopfield first showed for the case of error correction in the synthesis of biological macromolecules, thermodynamic equilibrium imposes fundamental limits—we have called them Hopfield barriers [14]—on the functional capacities of biological systems [33]. These limits can be exceeded only by the expenditure of energy. The need to account explicitly for the nonequilibrium nature of biological processes has been felt even more acutely in recent years, and understanding the implications of the breakdown of detailed balance has been central to this effort [14,16,34]. While detecting and measuring departure from equilibrium has become feasible in systems where mechanical work is done, as in observations of detailed-balance violations in the dynamics of bacterial flagella [35], it has proved more challenging for cellular information processing [36].

Cycle counting offers an alternative approach for analyzing nonequilibrium behavior which is becoming experimentally feasible. Advances in single-molecule experimental techniques are making it possible to observe in real time such processes as the conformational and binding behavior of enzymes [37], the processivity of molecular motors [38], and the binding and unbinding of transcription factors during gene regulation [39]. These developments hold out the tantalizing possibility that the results presented here could be used not only to confirm departure from thermodynamic equilibrium but also to identify the sources and quantify the extent of energy expenditure.

ACKNOWLEDGMENTS

The authors thank two anonymous reviewers for their constructive suggestions which led to several improvements in the exposition and Jeremy Owen and Chris Jarzynski for helpful comments on the results. J.W.B. and J.G. were supported by NSF Grant No. 1462629.

-
- [1] T. L. Hill, Studies in irreversible thermodynamics IV. Diagrammatic representation of steady state fluxes for unimolecular systems, *J. Theoret. Biol.* **10**, 442 (1966).
 - [2] J. Schnakenberg, Network theory of microscopic and macroscopic behavior of master equation systems, *Rev. Mod. Phys.* **48**, 571 (1976).
 - [3] C. Jarzynski, Nonequilibrium Equality for Free Energy Differences, *Phys. Rev. Lett.* **78**, 2690 (1997).
 - [4] G. E. Crooks, Entropy production fluctuation theorem and the nonequilibrium work relation for free energy differences, *Phys. Rev. E* **60**, 2721 (1999).
 - [5] G. Gallavotti and E. G. D. Cohen, Dynamical Ensembles in Nonequilibrium Statistical Mechanics, *Phys. Rev. Lett.* **74**, 2694 (1995).
 - [6] J. L. Lebowitz and H. Spohn, A Gallavotti-Cohen-type symmetry in the large deviation functional for stochastic dynamics, *J. Stat. Phys.* **95**, 333 (1999).
 - [7] D. Andrieux and P. Gaspard, Fluctuation theorem for currents and Schnakenberg network theory, *J. Stat. Phys.* **127**, 107 (2007).
 - [8] S. Rahav and C. Jarzynski, Fluctuation relations and coarse-graining, *J. Stat. Mech.* (2007) P09012.

- [9] U. Seifert, Stochastic thermodynamics: Principles and perspectives, *Eur. Phys. J. B* **64**, 423 (2008).
- [10] C. Van den Broeck and M. Esposito, Ensemble and trajectory thermodynamics: A brief introduction, *Physica A* **418**, 6 (2015).
- [11] J. Gunawardena, A linear framework for time-scale separation in nonlinear biochemical systems, *PLoS ONE* **7**, e36321 (2012).
- [12] F. Wong, A. Dutta, D. Chowdhury, and J. Gunawardena, Structural conditions on complex networks for the Michaelis-Menten input-output response, *Proc. Natl. Acad. Sci. USA* **115**, 9738 (2018).
- [13] I. Mirzaev and J. Gunawardena, Laplacian dynamics on general graphs, *Bull. Math. Biol.* **75**, 2118 (2013).
- [14] J. Estrada, F. Wong, A. DePace, and J. Gunawardena, Information integration and energy expenditure in gene regulation, *Cell* **166**, 234 (2016).
- [15] F. Wong, A. Amir, and J. Gunawardena, Energy-speed-accuracy relation in complex networks for biological discrimination, *Phys. Rev. E* **98**, 012420 (2018).
- [16] J. W. Biddle, M. Nguyen, and J. Gunawardena, Negative reciprocity, not ordered assembly, underlies the interaction of Sox2 and Oct4 on DNA, *eLife* **8**, e41017 (2019).
- [17] J. Gunawardena, Time-scale separation: Michaelis and Menten's old idea still bearing fruit, *FEBS J.* **281**, 473 (2014).
- [18] F. Wong and J. Gunawardena, Gene regulation in and out of equilibrium, *Annu. Rev. Biophys.* **49**, 199 (2020).
- [19] G. R. Ainslie, Jr., J. P. Shill, and K. E. Neet, Transients and cooperativity, *J. Biol. Chem.* **247**, 7088 (1972).
- [20] V. J. Hilser, J. A. Anderson, and H. N. Motlagh, Allostery vs. "allokairy," *Proc. Natl. Acad. Sci. USA* **112**, 11430 (2015).
- [21] W. T. Tutte, The dissection of equilateral triangles into equilateral triangles, *Proc. Cambridge Phil. Soc.* **44**, 463 (1948).
- [22] D. ter Haar, *Elements of Statistical Mechanics* (Reinhardt and Co., New York, 1954).
- [23] B. M. Mahan, Microscopic reversibility and detailed balance, *J. Chem. Ed.* **52**, 299 (1975).
- [24] U. Seifert, Stochastic thermodynamics of single enzymes and molecular motors, *Eur. Phys. J. E* **34**, 26 (2011).
- [25] M. Bauer and F. Cornu, Local detailed balance: A microscopic derivation, *J. Phys. A: Math. Theor.* **48**, 015008 (2015).
- [26] D. W. Stroock, *An Introduction to Markov Processes*, Graduate Texts in Mathematics Vol. 230 (Springer, Berlin, 2005).
- [27] See Supplemental Material at <http://link.aps.org/supplemental/10.1103/PhysRevE.101.062125> for details of the Gillespie simulations used for Fig. 3.
- [28] T. L. Hill, Free energy and the kinetics of biochemical diagrams, including active transport, *Biochemistry* **14**, 2127 (1975).
- [29] T. L. Hill and Y.-D. Chen, Stochastics of cycle completions (fluxes) in biochemical diagrams, *Proc. Natl. Acad. Sci. USA* **72**, 1291 (1975).
- [30] D.-Q. Jiang, M. Qian, and M.-P. Qian, *Mathematical Theory of Nonequilibrium Steady States: On the Frontier of Probability and Dynamical Systems*, Lecture Notes in Mathematics Vol. 1833 (Springer, Berlin, 2004).
- [31] R. García-García, V. Lecompte, A. B. Kolton, and D. Domínguez, Joint probability distributions and fluctuation theorems, *J. Stat. Mech.* (2012) P02009.
- [32] A. Wachtel, R. Rao, and M. Esposito, Thermodynamically consistent coarse graining of biocatalysts beyond Michaelis-Menten, *New J. Phys.* **20**, 042002 (2018).
- [33] J. J. Hopfield, Kinetic proofreading: A new mechanism for reducing errors in biosynthetic processes requiring high specificity, *Proc. Natl. Acad. Sci. USA* **71**, 4135 (1974).
- [34] Y. Tu, The nonequilibrium mechanism for ultrasensitivity in a biological switch: Sensing by Maxwell's demons, *Proc. Natl. Acad. Sci. USA* **105**, 11737 (2008).
- [35] C. Battle, C. P. Broedersz, N. Fakhri, V. F. Geyer, J. Howard, C. F. Schmidt, and F. C. MacKintosh, Broken detailed balance at mesoscopic scales in active biological systems, *Science* **352**, 604 (2016).
- [36] Q. Liu and J. Wang, Quantifying the flux as the driving force for nonequilibrium dynamics and thermodynamics in non-Michaelis-Menten enzyme kinetics, *Proc. Natl. Acad. Sci. USA* **117**, 923 (2020).
- [37] H. P. Lu, Sizing up single-molecule enzymatic conformational dynamics, *Chem. Soc. Rev.* **43**, 1118 (2014).
- [38] M. Sikor, K. Mapa, L. V. von Voithenberg, D. Mokranjac, and D. C. Lamb, Real-time observation of the conformational dynamics of mitochondrial Hsp70 by spFRET, *EMBO J.* **32**, 1639 (2013).
- [39] J. Chen, Z. Zhang, L. Li, B.-C. Chen, A. Revyakin, B. Hajj, W. Legand, M. Dahan, T. Lionnet, E. Betzig, R. Tjian, and Z. Liu, Single-molecule dynamics of enhanceosome assembly in embryonic stem cells, *Cell* **156**, 1274 (2014).

Supplemental Information for “Reversal symmetries for cyclic paths away from thermodynamic equilibrium”

John W. Biddle¹ and Jeremy Gunawardena¹

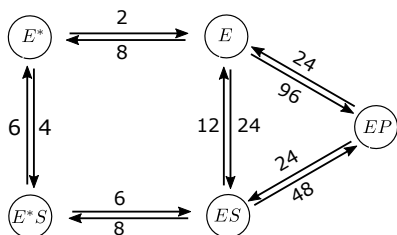
¹Department of Systems Biology, Harvard Medical School, Boston, United States

April 8, 2020

As discussed in the Paper, we carried out Gillespie simulations using the model shown in Paper Fig. 1 in order to illustrate the central result of the Paper. The outcome of the simulations is summarized in Paper Fig. 3. The length of the initial simulations was 3×10^6 timesteps, which was sufficient for all reversal ratios to converge, as well as for the net fluxes in cases (ii) and (iii) to converge. The net fluxes in case (i) did not converge satisfactorily in this time, however, so we extended the simulation to 1.2×10^7 timesteps, which was sufficient. We wrote the program to carry out the Gillespie simulations in Python, and it is available upon request.

Below, we present the rates, in arbitrary units with dimensions of $[\text{time}]^{-1}$, of each transition for each of the three scenarios described in the Paper. We also present the reciprocal temperature and the chemical potential difference(s) among the reservoirs. In each case the reciprocal temperature corresponds to $T = 298$ K.

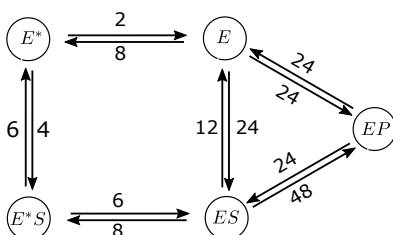
Case (i)



$$\beta = 0.404 \text{ mol/kJ}$$

$$\mu_P - \mu_S = 0$$

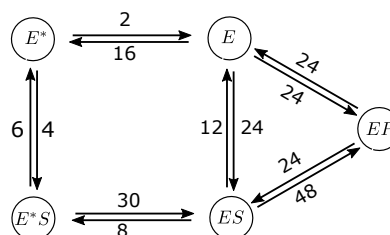
Case (ii)



$$\beta = 0.404 \text{ mol/kJ}$$

$$\mu_P - \mu_S = 3.43 \text{ kJ/mol}$$

Case (iii)



$$\beta = 0.404 \text{ mol/kJ}$$

$$\mu_P - \mu_S = 3.43 \text{ kJ/mol}$$

$$\mu_{\text{ATP}} - \mu_{\text{ADP}} - \mu_{\text{P}_i} = 5.70 \text{ kJ/mol}$$